OncoTargets and Therapy

Dovepress
Taylor & Francis Group

Open Access Full Text Article

ORIGINAL RESEARCH

Icariin Inhibits Lung Adenocarcinoma Progression Through TP53-Mediated Ferroptosis

Qihua Jin[1,2], Li OuYang[2], Jingjing Li[2], Xiaoxia Yang[3], Lihua Guo[1,3]

[1]The First Clinical Medical College, Nanjing University of Chinese Medicine, Nanjing, Jiangsu, People's Republic of China; [2]Department of TCM Respiratory, Yunnan Provincial Hospital of Traditional Chinese Medicine, The First Affiliated Hospital of Yunnan University of Traditional Chinese Medicine, Kunming, Yunnan, People's Republic of China; [3]Department of TCM Oncology, Yunnan Provincial Hospital of Traditional Chinese Medicine, The First Affiliated Hospital of Yunnan University of Traditional Chinese Medicine, Kunming, Yunnan, People's Republic of China

Correspondence: Lihua Guo, The First Clinical Medical College, Nanjing University of Chinese Medicine, Nanjing, Jiangsu, People's Republic of China, Email guolihua1101@qq.com

Purpose: Lung adenocarcinoma (LUAD) represents the predominant histological subtype of non-small cell lung cancer (NSCLC) and is linked to a diminished overall survival (OS) rate. Icariin (ICA), the principal bioactive compound found in the medicinal plant Epimedium, has demonstrated significant efficacy in inhibiting tumor progression. Ferroptosis, an emerging mechanism of cellular demise, offers a promising avenue for therapeutic intervention in oncology. Nonetheless, the function and modulation of ferroptosis in LUAD are still significantly under-investigated.

Methods: A potential ferroptosis target was identified via bioinformatics analysis. Levels of reactive oxygen species (ROS) and ferroptosis-associated markers were quantified, while MTT, wound healing (WH), and Transwell assays were conducted to assess the effect of ICA on the malignant behavior of the LUAD cell line A549. The antitumor activity of ICA was further validated in vivo. Additionally, transcriptome sequencing and bioinformatics analysis were performed to explore ICA-induced molecular regulatory changes associated with the malignant phenotype of tumors.

Results: Bioinformatics analysis revealed that TP53 is a potential target of ferroptosis. Cellular experiments demonstrated that ICA induces ferroptosis in a dose-dependent manner, significantly reducing the proliferation, migration, and invasion abilities of A549 cells. Furthermore, the ferroptosis inhibitor Fer-1 can partially reverse both the ferroptosis and the increased expression of TP53 induced by ICA, indicating that ICA suppresses the malignant behavior of A549 cells by inducing TP53-mediated ferroptosis. This mechanism of action was further validated by in vivo experiments. Additional transcriptome sequencing and bioinformatics analysis showed that the mechanism by which ICA inhibits the proliferation of lung cancer cells may be related to its effects on cell cycle and metastasis-related gene sets, lipid metabolism, tumor immune microenvironment, and tumor-promoting pathways, including cholesterol metabolism, cortisol synthesis and secretion, and the PI3K-Akt signaling pathway.

Conclusion: ICA demonstrates antitumor properties in LUAD via TP53-mediated ferroptosis, consequently suppressing cellular proliferation.

Keywords: lung adenocarcinoma, icariin, ferroptosis, TP53, immune cell

Introduction

Lung cancer (LC) ranks among the foremost contributors to cancer-related mortality on a global scale.[1] It is chiefly categorized into two main types: non-small cell lung cancer (NSCLC) and small cell lung cancer (SCLC). Notably, NSCLC represents around 85% of all LC instances, with LUAD identified as one of its most common subtypes.[2] Presently, treatment modalities for LUAD encompass surgery, chemotherapy, radiotherapy, targeted therapy, and immunotherapy.[3] Surgery remains the primary treatment for early-stage LUAD; however, localized LUAD can progress and invade adjacent structures such as the heart, large blood vessels, and trachea, rendering them unresectable and typically treated with chemotherapy and/or radiotherapy.[4] Unfortunately, chemotherapy is often associated with side effects, and radiotherapy can damage surrounding healthy tissues. Molecular targeted therapies are frequently employed for a specific group of LUAD patients, especially those who are younger and do not smoke. In cases of advanced NSCLC

Received: 10 May 2025
Accepted: 26 October 2025
Published: 15 November 2025

where patients do not respond to established molecular targeted therapies, the standard treatment approach generally involves a combination of platinum-based chemotherapy (either carboplatin or cisplatin paired with pemetrexed) and immunotherapy, irrespective of histological subtype or PD-L1 expression levels.[5] As a result, it is crucial to pinpoint safe and effective anticancer agents that are widely accessible and exhibit minimal side effects for the treatment of LUAD.

Recent studies have revealed the pivotal role of ferroptosis in antitumor mechanisms, and targeting ferroptosis-related pathways has emerged as a promising strategy for inhibiting tumor initiation and progression. Ferroptosis is a newly recognized form of programmed cell death, characterized by iron accumulation and the generation of lipid-derived reactive oxygen species (ROS).[6] Iron metabolism is an important cellular process in the occurrence of ferroptosis. During this process, the membrane protein transferrin receptor 1 (TFR1) transports $Fe3^+$ to the endosome, where it is reduced to $Fe2^+$. Divalent metal transporter 1 (DMT1) releases $Fe2^+$ from the endosome into the intracellular labile iron pool (LIP). Excess iron is stored in the cytoplasm as ferritin, composed of light chain (FTL) and ferritin heavy chain 1 (FTH1).[7,8] When iron metabolism is imbalanced, $Fe2^+$ undergoes a Fenton reaction with hydrogen peroxide, a product of mitochondrial oxidative respiration, generating $Fe3^+$ and ROS represented by hydroxyl radicals, which triggers the accumulation of lipid peroxides (LPO) and ultimately leads to ferroptosis.[9,10] An imbalance between ROS and the antioxidant defense system in tumor cells leads to excessive increase of ROS, inducing ferroptosis in tumor cells. Intracellular natural antioxidant mechanisms such as the cystine/glutamate antiporter system (System Xc-), glutathione-glutathione peroxidase 4 (GPX4) system, etc., can timely monitor and eliminate excessively high intracellular ROS and LPO, maintaining ferroptosis homeostasis.[11] Among them, System Xc^- consists of a light chain subunit (SLC7A11) and a heavy chain subunit (SLC3A2), and the System Xc^--glutathione-GPX4 axis plays a core role in limiting lipid peroxidation.[12] Therefore, the targeted regulation of key regulatory proteins in ferroptosis is a core link in inducing ferroptosis in tumor cells and thereby inhibiting their proliferation.

Agents that induce ferroptosis, such as sorafenib, sulfasalazine, statins, and artemisinin, show considerable potential in enhancing strategies for tumor treatment.[13] Preliminary findings suggest that statins could potentially improve OS rates in individuals diagnosed with various forms of cancer, including colorectal cancer.[14] Beyond these well-studied agents, natural bioactive compounds have also garnered attention for their anticancer properties, with increasing evidence highlighting their ability to modulate cell death pathways like ferroptosis. For example, dihydroartemisinin, dihydroisotanshinone, and gallic acid have been reported to exert anti-lung cancer effects by inducing ferroptosis.[15]

Icariin (ICA), the primary bioactive compound obtained from the medicinal plant Epimedium, demonstrates a diverse range of anticancer effects.[16,17] ICA has shown effectiveness in suppressing the advancement of multiple tumor types, such as breast cancer (BC),[18] colon cancer (CC),[19] ovarian cancer (OC),[20] hepatocellular carcinoma,[21] and LC.[22,23] Furthermore, ICA has the capability to trigger apoptosis in neoplastic cells.[24] ICA-curcumol has shown the capacity to trigger ferroptosis in prostate cancer (PC) cells via the Nrf2/HO-1 pathway.[25] Given these observations, ICA may serve as a potential inducer of ferroptosis in LC cells, warranting further investigation into its underlying mechanisms.

In this study, we identified TP53 as a potential target of ferroptosis in LUAD through bioinformatics analysis. Following this, we examined the effect of ICA on the biological characteristics of A549 cells utilizing MTT, WH, and Transwell assays. Our findings suggested that ICA demonstrated anti-tumor effects by promoting the process of ferroptosis. Additionally, RNA sequencing (RNA-seq) was conducted to investigate the transcriptomic changes induced by ICA. The results demonstrate that ICA can trigger ferroptosis in a manner that is dependent on dosage, while also inhibiting the proliferation, migration, and invasion of A549 cells. Further investigation into the anticancer properties of ICA confirmed the involvement of the ferroptosis pathway. The RNA-seq analysis demonstrated significant activation of Mø, NK T cells, CD4+ T cells, and CD8+ T cells, alongside the induction of metabolic dysregulation. The results indicate a new mechanism by which ICA influences ferroptosis in LUAD, presenting potential therapeutic avenues and enhanced treatment alternatives for patients with LUAD.

Materials and Methods

Data Collection and Processing

We utilized the R TCGAbiolinks (v 2.26.0) program to acquire the counts and clinical data, whereas the TCGA-LUAD FPKM expression data were obtained from UCSC Xena. The GSE72094 dataset was sourced from the GEO database. To

identify differentially expressed genes (DEGs) associated with ferroptosis, a p-value of less than 0.05 and a |log2 fold change| greater than 0.5 were utilized.

Molecular Docking

The crystal structure of the TP53 protein was downloaded from the PDB database (https://www.rcsb.org/), and the three-dimensional structure of the active ingredient was obtained from the PubChem database. The ligand molecule was subjected to energy minimization using ChemDraw (v23.1.1) software, and molecular docking was performed 20 times with AutoDock Vina. If the docking binding energy is less than −1.2 kcal/mol, the docking result is considered feasible.

Cell Culture

Cells from the Type Culture Collection at the Kunming Institute of Zoology of the China Academy of Sciences were used to cultivate human LUAD A549 cells. The cells were cultured on a 37°C plate in a 5% CO_2 incubator using RPMI-1640 medium (Gibco, USA) supplemented with 10% fetal bovine serum (FBS) (Bioind, Israel).

Cell Grouping and Treatment

To initially explore the potential biological effects of ICA on A549 cells, the cells were randomly divided into five groups: a control group, and ICA 10 μM, ICA 20 μM, ICA 40 μM, and ICA 80 μM groups.[26] The control group received the same treatment without ICA, whereas the remaining groups were treated with ICA at the corresponding concentrations for 24 h. Moreover, ICA (SML0551, Sigma-Aldrich, USA) was dissolved in dimethyl sulfoxide (DMSO; D8418, Sigma-Aldrich, USA) to prepare working solutions at concentrations of 10, 20, 40, and 80 μM.

In the rescue assays, A549 cells were seeded at a density of 3.5×10^5 cells/well and randomly divided into four groups: (1) Blank control group, in which cells were maintained in regular culture without ICA treatment; (2) Positive control group, in which cells were treated with 10 μM Erastin (MedChemExpress, China); (3) ICA group, in which cells were treated with 80 μM ICA for 24 h; and (4) ICA + Fer-1 group, in which cells were pretreated with 1 μM Ferrostatin-1 (Fer-1, Sigma-Aldrich, USA) for 60 min, followed by co-treatment with 80 μM ICA for 24 h.

Cell Proliferation Activity Assay

In 96-well plates, 1500 cells/well were used to seed A549 cells during their logarithmic development phase. For 0, 24, 48, and 72 hours, the treatment groups were subjected to varying doses of ICA (10, 20, 40, and 80 μM), whereas the control groups received the same treatment without ICA. Each group utilized five replicate wells. The serum-containing medium was substituted with serum-free media after treatment, and MTT reagent (ct02, Sigma-Aldrich) was added. Three hours later, the cells were placed in an incubator set at 37°C. Thermo Scientific's Evolution One spectrophotometer was used to measure the optical density (OD) at 450 nm, which is a measure of cell proliferation activity.

Wound-Healing (WH) and Transwell Assays

To conduct the WH assay, sterile pipette tips were used to scrape the surface of the culture plate in order to simulate wounds. Phosphate Buffer Saline (PBS) from Gibco, USA, was used twice to wash the cells and eliminate any cell debris. A total of 12 and 24 hours were spent incubating cells in the treatment groups with ICA (10, 20, 40, and 80 μM) at 37°C, whereas the control groups received the same treatments but without ICA. Observations were made of the wound edges' movement with an inverted microscope (Olympus, IX53, Japan), and the results were measured by measuring the distance between the wound edges.

For the Transwell assay, A549 cells that had been treated were left to migrate into a lower chamber for 24 hours. This chamber contained 0.8 mL of media with 10% FBS (Bioind, Israel). Subsequently, 0.4% crystal violet was used to stain the migratory cells on the membrane's lower surface, and photos were taken using a 100× magnification Olympus IX53 microscope from Japan.

Measurement of Intracellular ROS

Ten micrograms of DCFH-DA (MedChemExpress, China) was added to each treatment group's cells after cell collection for a duration of 20 minutes at 37°C. The cells were then treated with two washes of serum-free medium. The fluorescence signal was assessed using flow cytometry using a CytoFLEX flow cytometer (Beckman Coulter).

Quantitative Real-Time Polymerase Chain Reaction (RT-qPCR)

After subjecting A549 cells to various compounds, total RNA was extracted using TriQuick reagent (Solarbio, Cat#R1100, China). The RNA was converted to cDNA by reverse transcription using the MasterServicebio RT First Strand cDNA Synthesis Kit (Servicebio, Lot#YL203301, China) according to the manufacturer's instructions. For the study of messenger RNA, a qPCR master mix named 2xSYBR Green (Servicebio, China) was utilized. There was a 30-second dip to 95°C, followed by 40 cycles of 15°C and 30°C, to make up the thermal cycling conditions. Normalizing target gene expression to GAPDH levels allowed for the utilization of GAPDH as an internal control. Table 1 lists the primers that were utilized. The $2^{-\Delta\Delta Ct}$ technique was used to examine the qRT-PCR findings.

Western Blot (WB)

A lysis buffer called RIPA was used to extract and lyse the treated cells (Solarbio, R0010, China). Protein concentration was measured using the BCA protein assay. Then, SDS-PAGE gels (MDBio Inc., Lot #M221199, China) were loaded with the correct amounts of protein samples. The samples were moved on PVDF membranes (Millipore, Lot #K5NA8025F, USA) following electrophoresis. The membranes were treated with primary and secondary antibodies after a blocking step with 5% skim milk (BD, China). The main antibodies included anti-GPX4 (1:5000, ab125066), anti-ACSL4 (1:10000, ab155282), anti-FTH1 (1:2000, 11,682-1-AP), anti-P53 (5 μg/mL, ab26), anti-SLC7A11 (1:500, TD12509), anti-β-actin (1:20,000, 66,009-1-Ig), HRP-Goat Anti-rabbit IgG(H + L) (1:10000, SA00001–2) and HRP-Goat Anti-Mouse IgG(H+L) (1:10000, SA00001-1) antibody. The loading control was β-actin, and protein signals were identified with the help of ECL (Everbright Inc., ECLS6009, USA).

In vivo Tumor Model

A pathogen-free, optimally humid, and temperature-controlled environment was maintained for the male BALB/c nude mice that were purchased from Beijing Vital River Laboratory Animal Technology Co., Ltd. (China). At fifteen grams each, they were about seven to eight weeks old. The Animal Ethics Review Committee at Yunnan University of Traditional Chinese Medicine approved the animal research. Subcutaneous injection of 0.2 mL of an LC cell solution (1×10^7/mL) into the right axilla of male BALB/c mice was used to construct the tumor model. Three days following injection, the mice were randomly divided into four groups, with six mice in each group: NC, CIS, ICA, and CIS+ICA. Cisplatin was administered to the positive control group by MERCK, Germany. The course of treatment began on day 3 and ended on day 20. The cisplatin group had an injection of 0.1 mg/d, the ICA group got 70 mg/kg/d of ICA gavaged,

Table 1 Primers Sequence for RT- qPCR

Gene	Forward Primer	Reverse Primer
GPX4	CAGTGAGGCAAGACCGAAGT	CCGAACTGGTTACACGGGAA
ACSL4	GGTTCGATTAAGCCCAGAGCC	GGTAATGGTTCCTCAGCTCCT
FTH1	AGCTCTACGCCTCCTACGTT	AAGGAAGATTCGGCCACCTC
TP53	TTGGAACTCAAGGATGCCCAG	TTATGGCGGGAGGTAGACTGA
SLC7A11	GCAAGCACACTCCTCTACCA	GGACGATGCATATCTGGGCA
EGFR	ACGAGTAACAAGCTCACGCA	CCAAGGACCACCTCACAGTT
KRAS	GGCAAGAGTGCCTTGACGA	CCTCTTGACCTGCTGTGTCG
NRAS	ATACATGAGGACAGGCGAAGG	TACTCGCTTAATCTGCTCCCTG
BRAF	GCCTCGGACTCTATTGGGC	TTCATCTGCTGGTCGGAAGG
PIK3CA	TAGGCAAGTCGAGGCAATGG	CTGGTCGCCTCATTTGCTCA
GAPDH	CTGGGCTACACTGAGCACC	AAGTGGTCGTTGAGGGCAATG

the CIS+ICA group got both cisplatin and ICA, and the NC group got an identical volume of 0.9% NaCl solution injected intraperitoneally. As soon as the tumors attained a size of 5×5 mm, they were evaluated every three days for tumor volume. Under ether anesthesia, malignancies were removed and weighed on day 21. For preservation, half of the tumors were placed in 10% formalin and the other half were frozen at −80°C.

Immunohistochemistry

The fixed tumor tissues were sectioned after being embedded in paraffin. The sections were deparaffinized and rehydrated before the antigen retrieval process using sodium citrate solution. Primary antibodies were added to the sections after an hour of incubation with 10% goat serum, and then they were left to incubate at 4°C overnight. The primary antibodies used were those produced by Affinity Biosciences Ltd. in Australia, and they were directed against GPX4, ACL4, and FTH1. The steps that followed were carbon copies of the manufacturer's original instructions.

Sequencing of Transcriptome and Bioinformatics Analysis

To isolate messenger RNA (mRNA), oligo(dT) beads were utilized, and total RNA was extracted from tumor tissues using the TriQuick reagent (Solarbio, China). To build libraries, we used NEB's NEBNext® Ultra™ RNA Library Prep Kit for Illumina® (NEB, USA) and reverse transcription to transform the messenger RNA (mRNA) into complementary DNA (cDNA). The NovaseqTM 6000 platform (Illumina, USA) was used by Novogene Co., Ltd. to conduct paired-end sequencing (2×150bp). By utilizing Hisat2 (v2.1.0) to align the raw data with the reference genome, clean reads were obtained. We used HTSeq v0.6.1 to quantify the mapping reads for every gene.[27] Both the length and the quantity of mapped reads were used to determine the FPKM values. The DESeq2 program in R (v4.0.4) was used to identify DEGs.[28] The p-values were adjusted according to the procedure suggested by Benjamini and Hochberg to account for the false discovery rate (FDR). Our criteria for selecting DEGs were a p-value below 0.05 and a |log2 (fold change)| above 1. To conduct functional enrichment analysis, with a significance level of $p< 0.05$, the KOBAS (bioinfo.org) web tools were utilized.[29] The results of the enrichment were shown using the R aPEAR (v1.0.0) package.[30]

In order to analyze pathways associated to metabolism and immune cell infiltration, the R GSVA package (v1.46.0) based on an RNA-seq expression matrix was used, together with the CIBERSORT and ssGSEA algorithms.[31] Using the CIBERSORT method, we compared the four groups' immunocyte infiltration status on 22 different subunits.[32] The ssGSEA technique was used to evaluate the infiltration scores of 28 immune cells using single-sample gene set enrichment analysis.

Statistical Analysis

Categorical data were presented as numerical values (percentage), while continuous data were delineated as mean ± SD. Statistical comparisons were executed through ANOVA. Statistical analysis of all bioinformatics data was performed using R version 2.26.0, while experimental data were analyzed with GraphPad Prism 9.5. Significance was established at a p value < 0.05. In the graphical representations, significance levels were denoted as follows: $*p < 0.05$, $**p < 0.01$, $***p < 0.001$, and $****p < 0.0001$.

Results

TP53 is a Potential Target of Ferroptosis in LUAD

To investigate the correlation between genes associated with ferroptosis and lung adenocarcinoma (LUAD) tumor tissues, we employed the TCGA-LUAD dataset to obtain the levels of these specific genes. 257 DEGs related to ferroptosis were identified when comparing LUAD tumor tissues to normal controls, utilizing the DESeq2 package for analysis. The heatmap illustrated a notable difference in expression, with the majority of genes exhibiting upregulation in the tumor tissues (Figure 1a). An analysis of the protein interaction network illustrated the relationships among 257 genes. TP53 was central to the regulatory network (Figure 1b), indicating that TP53 is crucial in the process of ferroptosis. We conducted additional validation of the relationship between TP53 and ferroptosis using various databases related to LUAD. The findings indicated a notable positive correlation between TP53 and the ferroptosis gene set observed in the

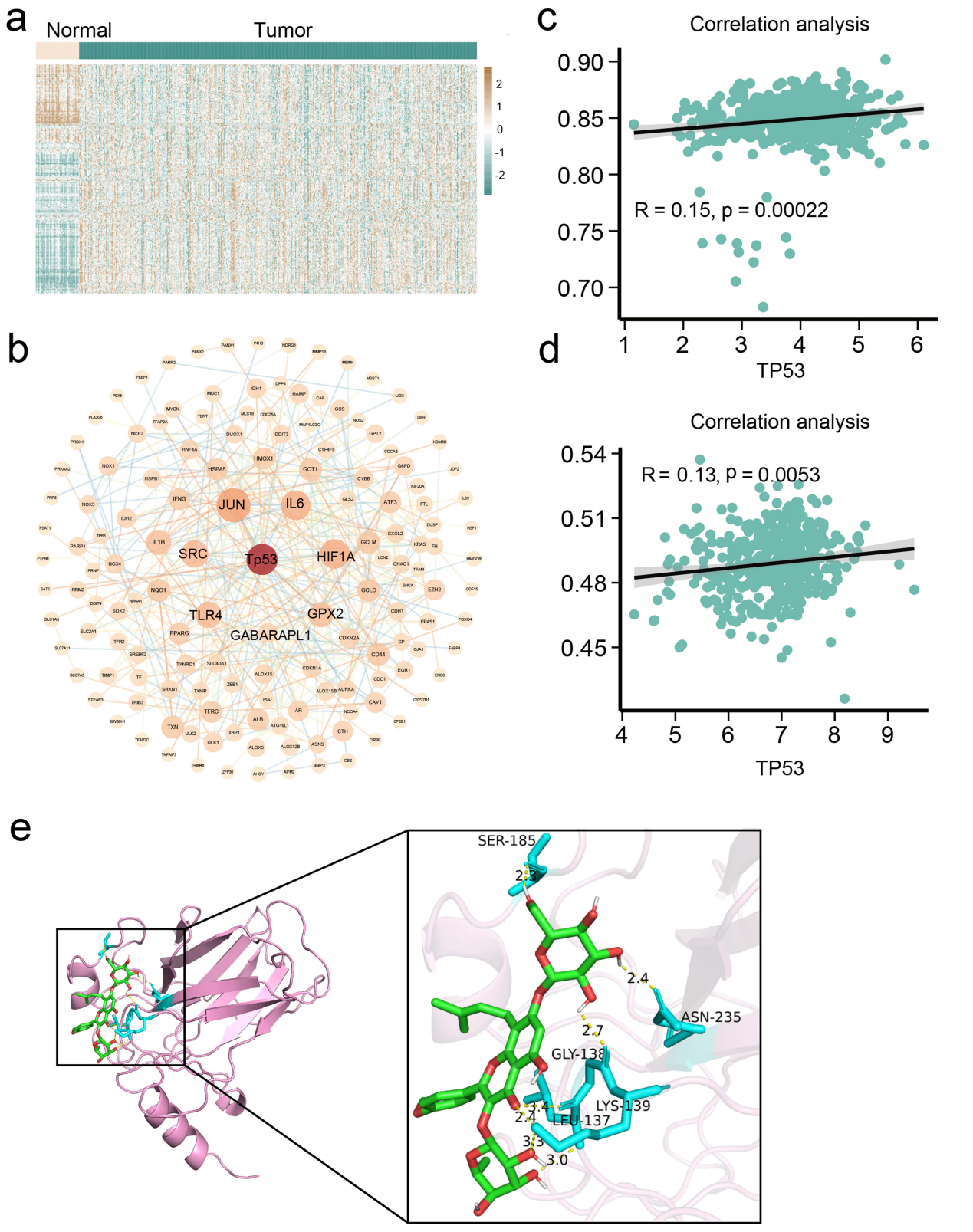

Figure 1 The correlation between TP53 and ferroptosis-related genes in lung adenocarcinoma (LUAD). (**a**) The expression heatmap of ferroptosis-related Differentially Expressed Genes (DEGs) in LUAD and adjacent normal tissues. (**b**) Protein-Protein Interaction (PPI) network analysis of differentially expressed ferroptosis-related genes (combined score > 0.8). (**c** and **d**) Correlation analysis between TP53 and ferroptosis gene set in TCGA-LUAD (**c**) and GEO (accession number: GSE72094) (**d**) database. (**e**) Molecular docking results of icariin and TP53. The green cyclic model represents icariin. The nearby cyan stick structures are amino acid residues that form hydrogen bond interactions with this active molecule, specifically including SER-185, ASN-235, GLY138, LYS-139, and LEU137 residues. A total of seven hydrogen bonds (marked by yellow dashed lines) are formed between these residues and the icariin molecule.

TCGA-LUAD and GSE72094 datasets (Figure 1c and d). Consequently, we hypothesize that TP53 may serve as a potential target for ferroptosis in LUAD. Furthermore, molecular docking analysis revealed a binding affinity of −7.4 kcal/mol between icariin and the target protein (Figure 1e). The results indicate that there is a stable interaction between icariin and the target protein: multiple amino acid residues participate in the binding through hydrogen bonds, and the relatively low docking affinity (far below the threshold of −1.2 kcal/mol) suggests a strong binding ability between the two.

ICA Inhibits Proliferation, Migration and Invasion of A549 Cells

To begin investigating the potential biological effects of ICA on A549 cells, we first tested how various doses of ICA (10, 20, 40, and 80 μM) affected the cells' capacity to survive for 24, 48, and 72 hours. ICA reduced cell viability after 72 hours in a dose-dependent manner, according to MTT experiments (Supplementary Figure S1a). Concentrations of 20, 40, and 80 μM of ICA significantly reduced the migration and invasion of A549 cells compared to the untreated controls, according to the results of the WH and Transwell tests ($p < 0.05$; Supplementary Figure S1b and c). The results indicate that ICA inhibits A549 cell growth, migration, and invasion.

ICA Induces Ferroptosis in A549 Cells

The overproduction of intracellular ROS is a defining characteristic of ferroptosis. We quantified the levels of ROS in A549 cells subjected to different concentrations of ICA. The findings indicated that concentrations of 10, 20, 40, and 80 μM ICA led to a notable elevation in ROS levels when compared to the control group ($p < 0.05$, Figure 2a and b). Additionally, the levels of ROS exhibited a dose-dependent increase corresponding to elevated concentrations of ICA (Figure 2b). Significant alterations in the expression levels of ferroptosis markers (GPX4, ACSL4, and FTH1) were noted following ICA treatment ($p < 0.05$, Figure 2c–e). The analyses conducted through qRT-PCR and WB demonstrated an increase in the mRNA and levels of ACSL4 in A549 cells treated with ICA, while the expression of SLC7A11 and GPX4 showed a decline (Figure 2c–e). ACSL4 expression demonstrated a marked dose-dependent increase ($p < 0.01$; Figure 2c). Nevertheless, the levels of GPX4 and FTH1 exhibited a significant reduction in a dose-dependent manner only when ICA treatment surpassed 20 μM ($p < 0.01$; Figure 2c). The combined presence of ROS, diminished levels of GPX4 and FTH1, alongside elevated ACSL4 expression, indicates that ICA triggers ferroptosis. Given that TP53 may serve as a target for ferroptosis and SLC7A11 plays a role in shielding cancer cells from oxidative stress.[33] We assessed the levels of TP53 and SLC7A11. The administration of ICA at concentrations of 20, 40, and 80 μM resulted in a notable increase in TP53 expression ($p < 0.001$) and a decrease in SLC7A11 levels ($p < 0.01$) (Figure 2d). Furthermore, the ICA treatment resulted in a downregulation of SLC7A11 protein expression, while there was an upregulation of TP53 expression (Figure 2e and f). The results indicate that TP53 could be essential in modulating ICA-induced ferroptosis within A549 cells.

ICA Inhibits A549 Cell Progression by Inducing the Ferroptosis Pathway

To investigate the inhibitory effect of ICA on A549 cells and its potential involvement in the ferroptosis pathway, we conducted rescue assays utilizing Fer-1, a recognized inhibitor of ferroptosis. MTT assays indicated that both the ICA and Erastin treatments led to a significant decrease in cell viability at the 24, 48, and 72-hour marks ($p < 0.01$). The analysis revealed no notable variation in cell viability between the ICA-treated cells and the negative control group following treatment with Fer-1, indicating that Fer-1 effectively counteracted the suppressive influence of ICA on cell proliferation (Figure 3a). The results from WH and Transwell assays demonstrated that the ICA group markedly decreased cell invasion and migration ($p < 0.05$). In contrast, Fer-1 was found to counteract the ICA-induced decrease in cell migration and invasion abilities (Figure 3b-c, Supplementary Figure S2a and b). We also measured ferroptosis indicators including GPX4, ACSL4, and FTH1, as well as intracellular ROS levels and the expression of driver genes linked to lung cancer, including EGFR, KRAS, NRAS, BRAF, and PIK3CA. The levels of ROS were significantly higher in the ICA and Erastin groups ($p < 0.01$, Figure 3d and e). In contrast, the levels of ROS were markedly diminished in Fer-1-treated ICA cells when juxtaposed with those receiving ICA treatment alone (Figure 3d and e). WB analysis demonstrated that Fer-1 altered the levels of GPX4, ACSL4, and FTH1 that were noted in the ICA and Erastin groups

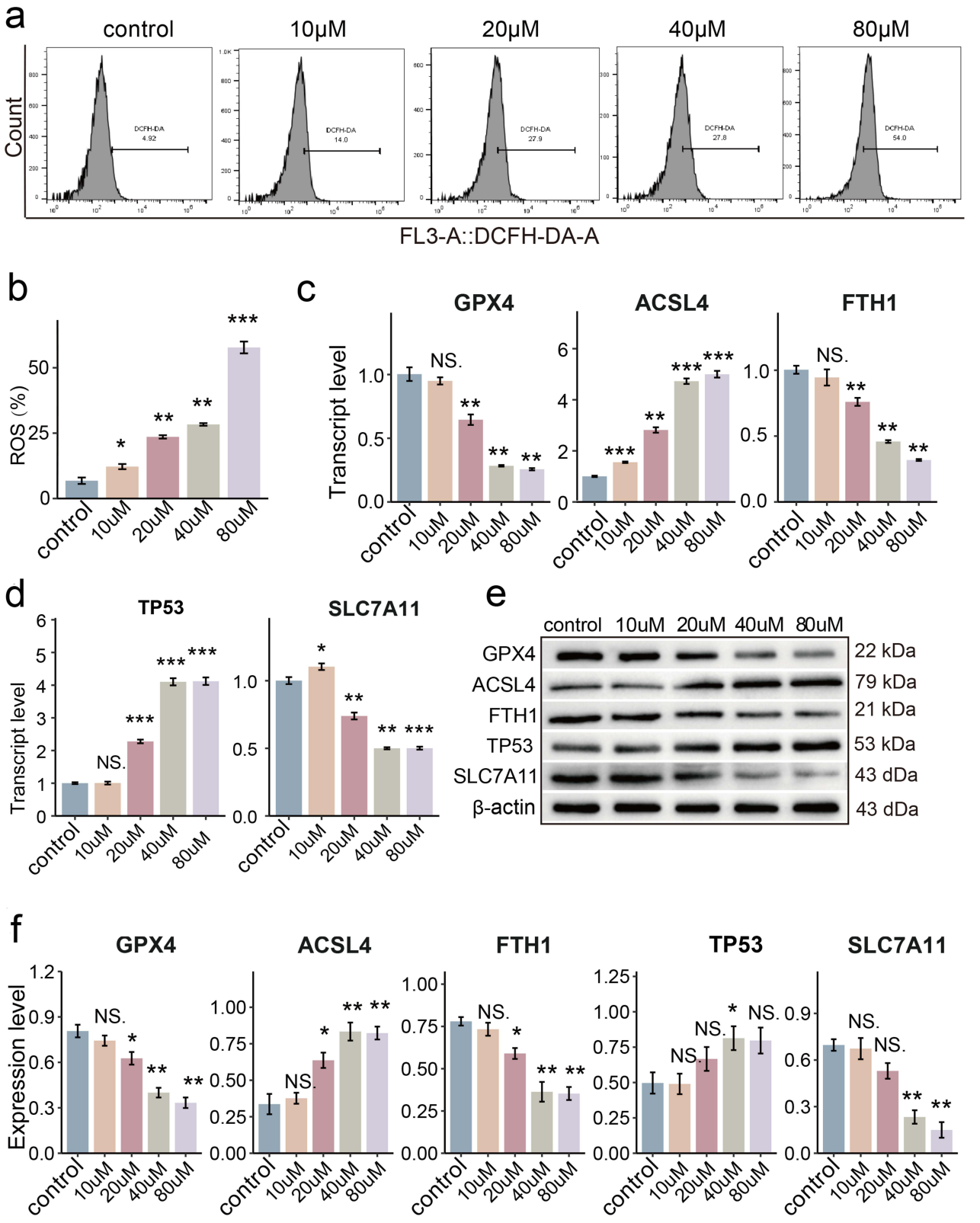

Figure 2 Icariin (ICA) induces ferroptosis in A549 cells. (**a** and **b**) Reactive Oxygen Species (ROS) levels in A549 cells with or without ICA treatment. (**c**) mRNA levels of GPX4, ACSL4, and FTH1 following ICA treatment. (**d**) mRNA levels of TP53 and SLC7A11 after ICA treatment. (**e** and **f**) Protein expression levels of ferroptosis-related genes following ICA treatment. *p<0.05, **p<0.01, or ***p<0.001 indicates significant difference compared with the control group.
Abbreviation: NS, no significant difference.

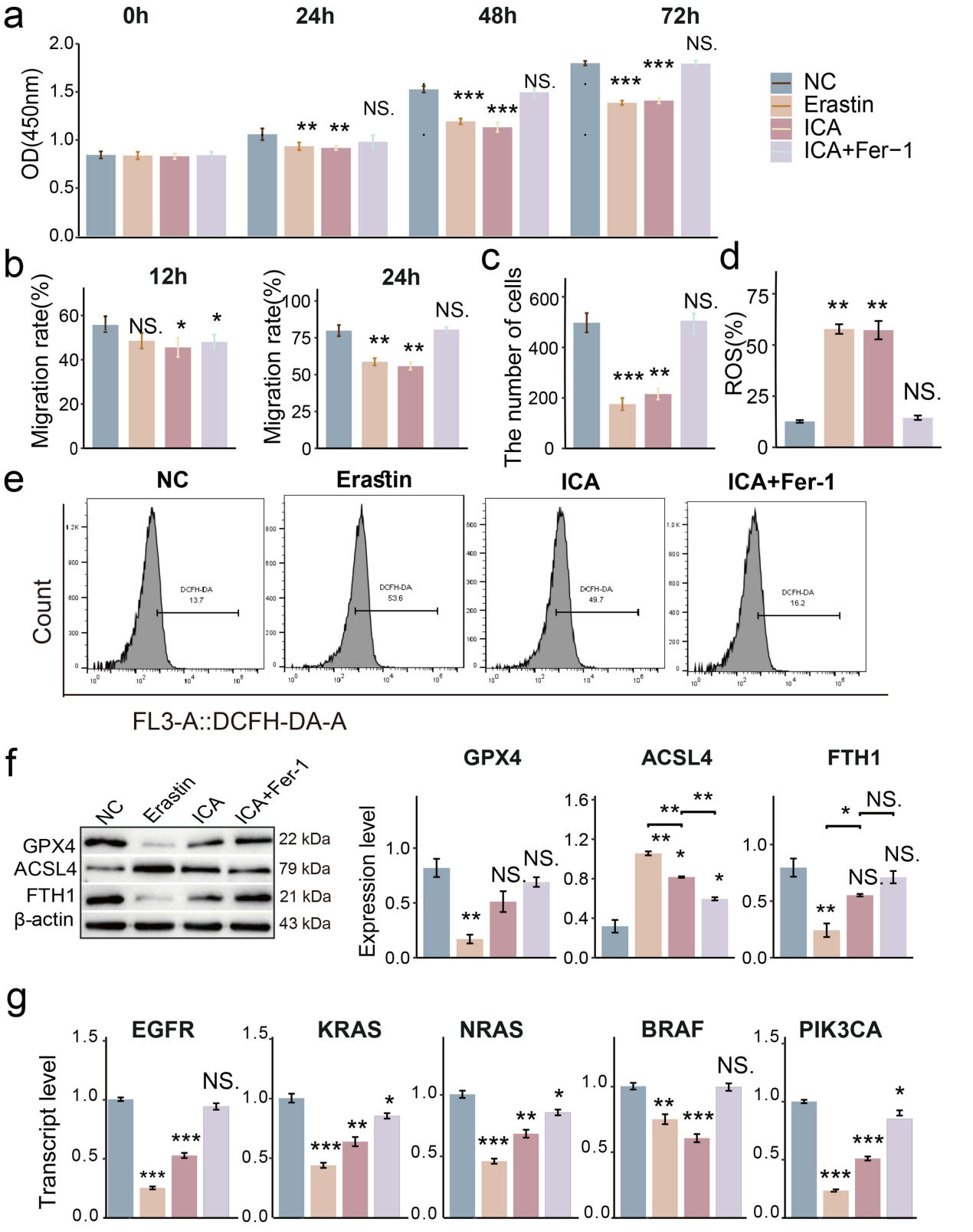

Figure 3 ICA inhibits A549 cells by the ferroptosis pathway. (**a**) The impact of Fer-1 on the inhibition of A549 cell proliferation induced by ICA. (**b** and **c**) The impact of Fer-1 on the inhibition of A549 cell migration (**b**) and invasion (**c**) induced by ICA. (**d** and **e**) The impact of Fer-1 on the increase of intracellular ROS levels induced by ICA. (**f**) The impact of Fer-1 on the expression of protein associated with ferroptosis, as influenced by ICA, is noteworthy. (**g**) The impact of Fer-1 on the expression levels of LUAD driver genes influenced by ICA. The cellular samples were categorized into four distinct groups: the negative control group, the positive control group treated with Erastin at a concentration of 10 μM, the ICA group receiving 80 μM of ICA, and the rescue assay group which consisted of ICA at 80 μM combined with Fer-1 at a concentration of 1 μmol/L. *p<0.05, **p<0.01, or ***p<0.001 indicates significant difference compared with the NC group.

Abbreviation: NS, no significant difference.

https://doi.org/10.2147/OTT.S539483

(Figure 3f). Additionally, Fer-1 notably counteracted the ICA-induced decrease in EGFR, KRAS, NRAS, BRAF, and PIK3CA ($p < 0.05$, Figure 3g). The findings collectively suggest that ICA influences A549 cells' cancerous behavior by activating the ferroptosis pathway and concurrently suppressing the expression of genes associated with tumor progression.

ICA Exerts Anti-Tumor Effects in vivo by Inducing Ferroptosis

To evaluate the anti-tumor efficacy of ICA, both independently and in conjunction with cisplatin (CIS), we developed a Lewis LC mouse model for in vivo studies. The treatments involving CIS and ICA demonstrated a marked reduction in tumor growth when contrasted with the NC group, with the combination of CIS and ICA exhibiting a more pronounced inhibitory effect than either treatment administered independently (Figure 4a). We conducted additional research to determine if ICA suppressed tumor growth by promoting ferroptosis. The findings demonstrated that the CIS+ICA group showed a notable decrease in the expression of GPX4 and FTH1, whereas ACSL4 was markedly increased ($p < 0.01$; Figure 4b). Furthermore, we examined the impact of CIS+ICA on genes associated with ferroptosis (Figure 4c and d, Supplementary Figure S3a). At the molecular and protein levels, CIS and ICA therapy increased TP53 expression while decreasing SLC7A11 expression. This suggests that ferroptosis is enhanced by CIS and ICA together through TP53 regulation (Figure 4e and f, Supplementary Figure S3b). Based on the findings, it appears that the interaction between CIS and ICA significantly reduces tumor growth by triggering ferroptosis. Furthermore, the expression levels of LUAD driver genes, including EGFR, KRAS, NRAS, BRAF, and PIK3CA, were evaluated in tumor tissues. Aside from BRAF, there was a notable decrease in the levels of EGFR, KRAS, NRAS, and PIK3CA within the CIS+ICA group, indicating a more extensive influence on tumor proliferation ($p < 0.01$; Figure 4g). In summary, these findings bolster the hypothesis that the interplay between CIS and ICA not only modulates genes associated with ferroptosis but also influences the expression of driver genes in LUAD.

Differential Gene Analysis and Functional Analysis

The principal component analysis (PCA) of RNA sequencing showed 40.9% differences in the PC1 axis and 21.08% differences in the PC2 axis, suggesting an obvious difference among CIS, ICA, CIS+ICA, and NC groups (Figure 5a). A total of 449 DEGs were identified in the CIS group, with 228 upregulated and 221 downregulated. Additionally, 656 DEGs (375 upregulated and 281 downregulated) were identified in the ICA versus NC comparison, and 518 DEGs (259 upregulated and 259 downregulated) were found in the CIS+ICA versus NC group (Figure 5b and Supplementary Table S1). Notably, there were 27 DEGs common to all three comparison groups (Figure 5c). KEGG pathway analysis revealed that the DEGs from the CIS versus NC, ICA versus NC, and CIS+ICA versus NC groups were enriched in different biological pathways (Figure 5d–f). In the CIS versus NC comparison, significant enrichment was found in pathways such as cholesterol metabolism, bile secretion, arginine and proline metabolism, intestinal immune network for IgA production, cortisol synthesis and secretion, and the PI3K-Akt pathway. In the ICA versus NC comparison, significant enrichment was observed in the estrogen signaling pathway, ether lipid metabolism, and phenylalanine metabolism. For the CIS+ICA versus NC comparison, key pathways included fatty acid biosynthesis, sphingolipid metabolism, Ras signaling, and Rap1 signaling. In conclusion, ICA mainly affected lipid metabolism and tumor-promoting related pathways, such as cholesterol metabolism, cortisol synthesis and secretion, and PI3K-Akt signaling pathway.

Immune Infiltration Analysis

To assess the infiltration of immune cells among the four groups, we utilized the CIBERSORT and ssGSEA algorithms (Figure 6a and b). The analysis performed with CIBERSORT revealed significant reductions in CD8 T cells among the CIS, ICA, and CIS+ICA groups. In contrast, there were noted elevations in CD4 memory resting T cells, activated NK cells, naive B cells, and Mø specifically within the CIS and ICA groups (Figure 6a). Notably, the CIS+ICA group demonstrated an increase in the specificity of memory B cells (Figure 6a). The ssGSEA results indicated significant increases in neutrophils, CD56dim NK cells, activated CD8 T cells, Mø, activated CD4 T cells, regulatory T cells, and NKT cells within both the CIS and ICA cohorts (Figure 6b). Ultimately, we evaluated the alterations in metabolism-associated KEGG pathways. The heatmap of ssGSEA scores indicated an upregulation of selenocompound metabolism in the CIS and ICA groups (Figure 6c). In contrast, the processes of fatty acid degradation, folate one-carbon metabolism,

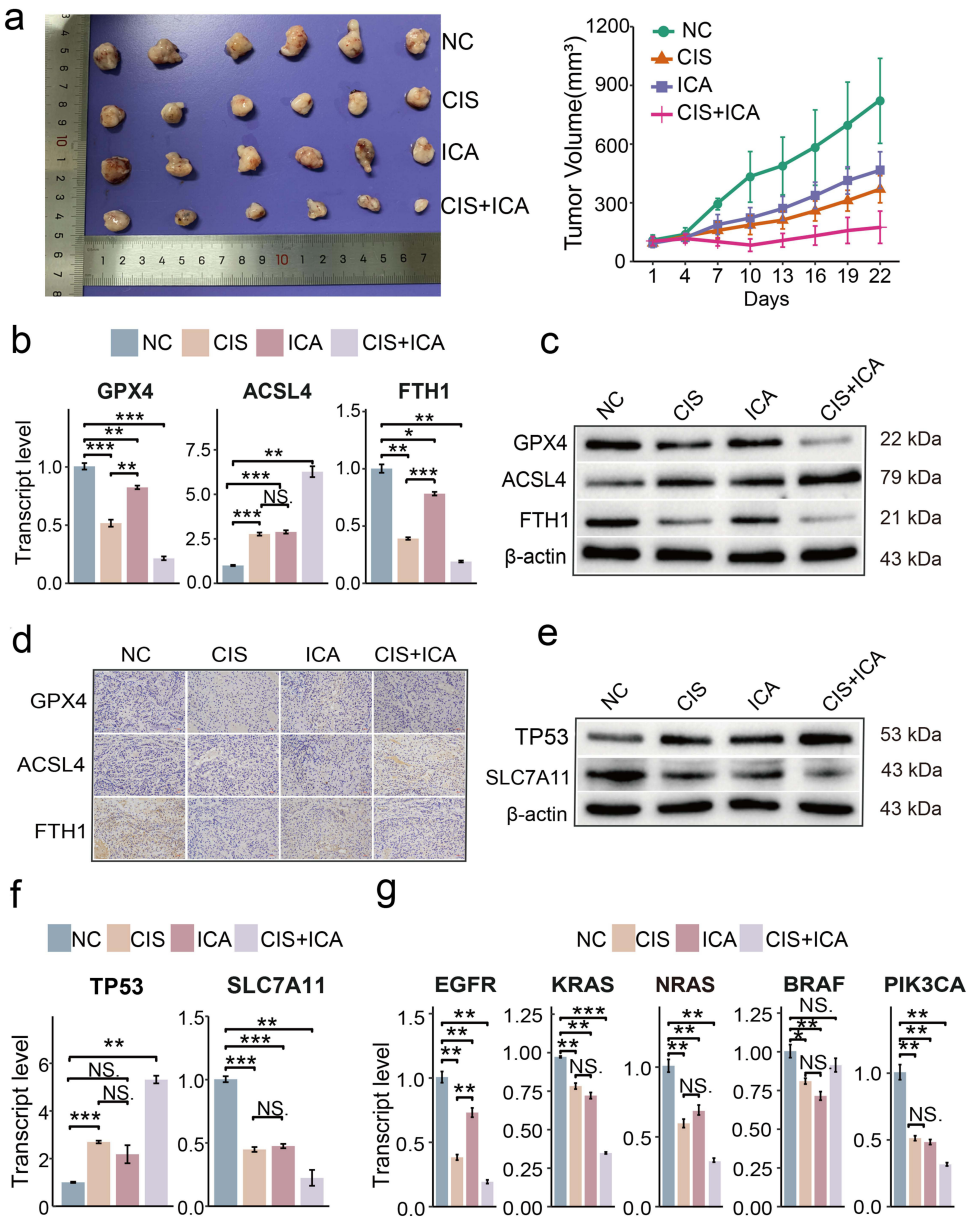

Figure 4 ICA exerts anti-tumor effects in vivo by inducing ferroptosis. (n=6) (**a**) The effects of ICA on tumor inhibition, both independently and in conjunction with cisplatin (CIS). (**b**) The impact of ICA, either independently or in conjunction with CIS, on the transcriptional expression of ferroptosis-related genes GPX4, ACSL4, and FTH1. (**c**) The regulatory impacts of ICA, either independently or in conjunction with CIS, on the protein expression levels of genes associated with ferroptosis, specifically GPX4, ACSL4, and FTH1. (**d**) The regulatory effects of ICA, either independently or in conjunction with CIS, on the expression levels of ferroptosis-related genes GPX4, ACSL4, and FTH1 were examined through immunohistochemistry (Scale bar =50μm). (**e** and **f**) The impact of ICA, both independently and in conjunction with CIS, on the protein and mRNA expression levels of TP53 and SLC7A11. (**g**) The regulatory impacts of ICA, whether administered alone or in conjunction with CIS, on the expression levels of driver genes associated with LUAD. *p<0.05, **p<0.01, or ***p<0.001 indicates significant difference compared with the NC group.
Abbreviation: NS, no significant difference.

various forms of O glycan biosynthesis, and glycosphosphatidylinositol biosynthesis exhibited suppression in the ICA and CIS+ICA groups. Meanwhile, steroid hormone biosynthesis, along with drug metabolism facilitated by other enzymes and cytochrome P450, showed activation in the CIS+ICA group (Figure 6c). The results indicate that both CIS and ICA treatments lead to an elevation in activated CD8 T cells, Mø, activated CD4 T cells, regulatory T cells, and NKT cells, accompanied by notable metabolic changes.

https://doi.org/10.2147/OTT.S539483

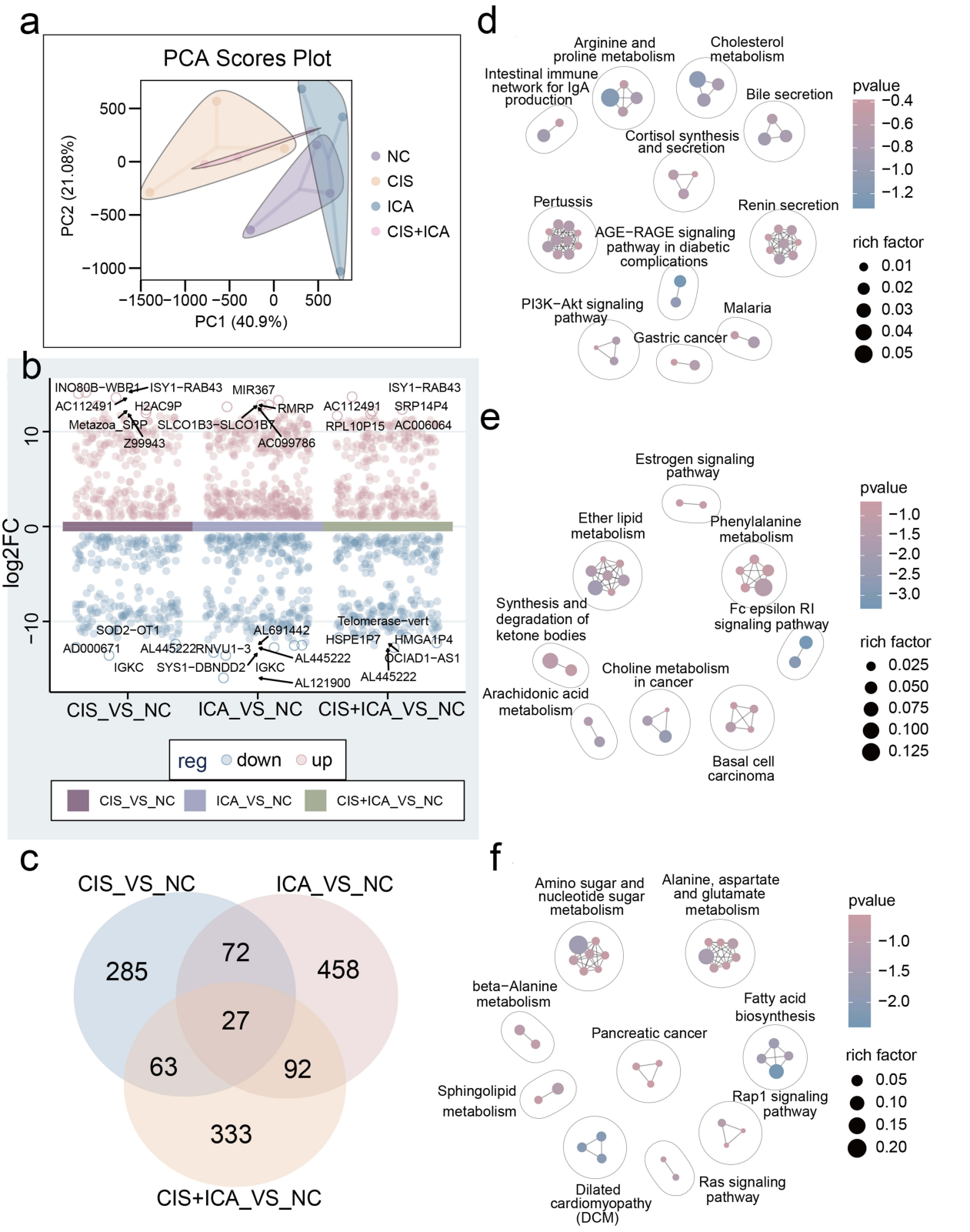

Figure 5 Transcriptome sequencing results. (**a**) PCA map of identified genes in all samples. (**b**) Volcano plots of DEGs. The most significantly upregulated and downregulated DEGs with the highest fold changes are labeled by black colored arrows in the plot for easy identification. (**c**) Venn plot of DEGs. d-f. KEGG transcriptome annotation results of DEGs in CIS vs NC (**d**), ICA vs NC (**e**), CIS+ICA vs NC (**f**).

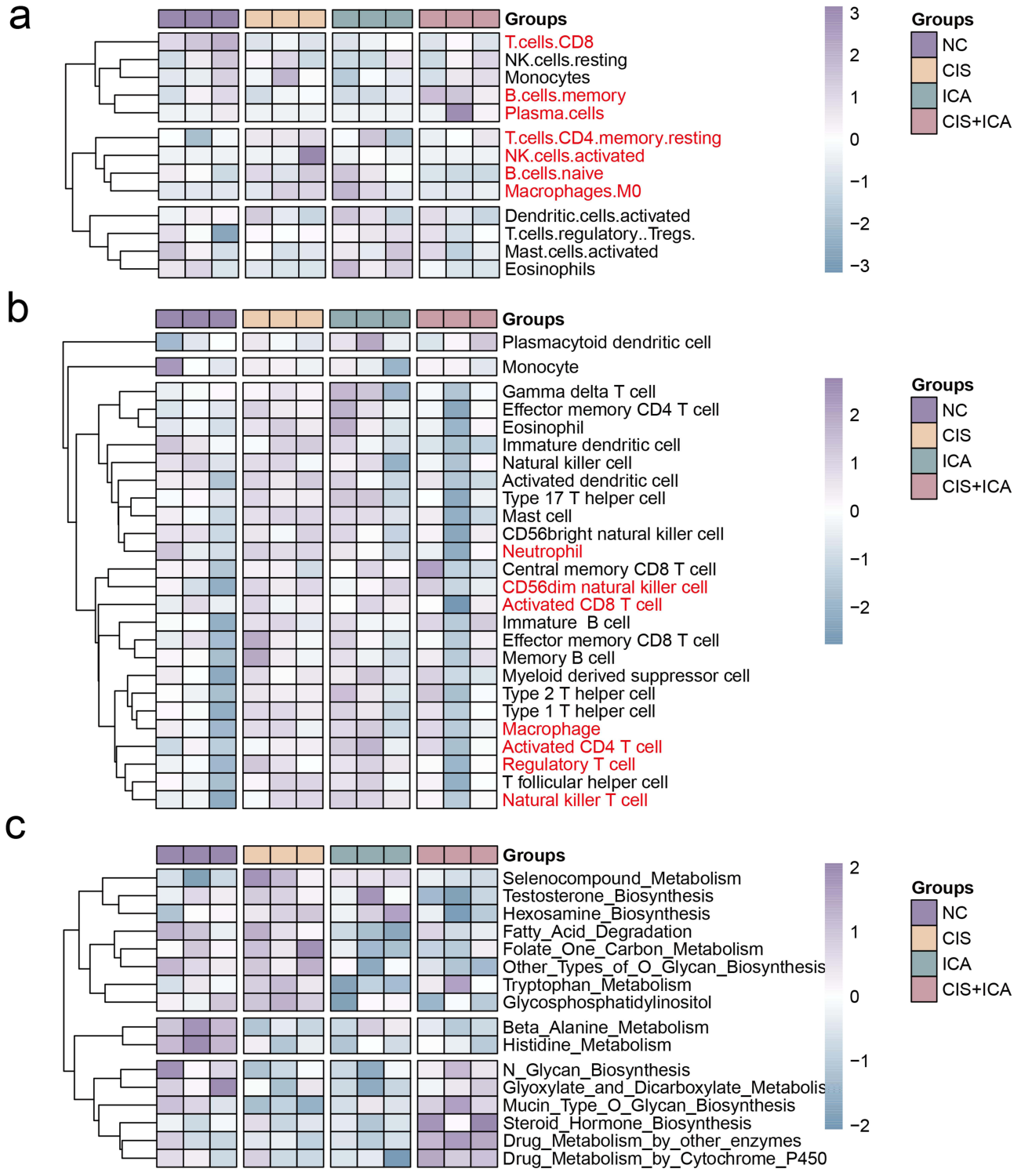

Figure 6 Immune and metabolism-related analyses result. (**a**) Immune cell infiltration in the four groups, predicted by CIBERSORT. The red-colored text indicates that there are significant differences in immune cells between groups. (**b**) Heatmap of ssGSEA scores related to 28 immune cell gene-set signatures. The red-colored text indicates that there are significant differences in immune cells between groups. (**c**) Heatmap of ssGSEA scores related to metabolism-related KEGG gene-set signatures.

Correlation Analysis Between Ferroptosis-Related Genes and Cell Function

After adding CIS/ICA/CIS +ICA, significant changes occurred in the ferroptosis-related genes and the proliferation, migration, and invasion of A549 cells. We discussed the relation between the five ferroptosis-related genes and cell

https://doi.org/10.2147/OTT.S539483

cycle-related or cell metastasis-related gene sets, and observed that SLC7A11 exhibited significant positive correlation with cell cycle-related genes sets (EGUCHI-CELL-CYCLE-RB1-TARGETS, REACTOME-APC-C-MEDIATED-DEGRADATION-OF-CELL-CYCLE-PROTEINS, GEORGES-CELL-CYCLE-MIR192-TARGETS, REACTOME-CELL-CYCLE-MITOTIC, CELL-CYCLE), whereas GPX4 showed a negative correlation with CELL-CYCLE (Supplementary Figure S4a). GPX4 was positively correlated with RAMASWAMY-METASTASIS-DN and LEE-METASTASIS-AND-ALTERNATIVE-SPLICING-UP, and significantly negatively correlated with the three gene sets (RICKMAN-METASTASIS-UP, BIDUS-METASTASIS-UP, WANG-METASTASIS-OF-BREAST-CANCER-ESR1-UP). Moreover, ACSL4, SLC7A11, and FTH1 exhibited significant negative correlations with most cell metastasis-related gene sets (Supplementary Figure S4b). These results explained the possible mechanisms by which ICA inhibits cell growth and metastasis. ICA may influence cell cycle and metastasis gene sets by regulating FTH1, SLC7A11, ACSL4, GPX4, TP53.

Discussion

Currently, despite advances in immunotherapy and targeted therapy, the prognosis for metastatic or recurrent LUAD remains unsatisfactory.[34] The pathogenesis of LUAD and the identification of novel strategies to reduce cancer mortality remain critical areas of research. The findings of our research indicate that ICA markedly reduced the proliferation, migration, and invasion of A549 cells in a manner that is dependent on the dosage administered. Furthermore, the application of ICA treatment resulted in the induction of ferroptosis within A549 cells. Both in vitro and in vivo studies demonstrated that ICA exerted its anti-tumor effects on LUAD through the upregulation of TP53-mediated ferroptosis. The results of RNA sequencing indicated that ICA predominantly influenced lipid metabolism and pathways associated with tumor promotion, such as cholesterol metabolism, cortisol synthesis and secretion, and the PI3K-Akt pathway. Furthermore, ICA enhanced the activity of Mø, NK T cells, CD4+ T cells, and CD8+ T cells. In summary, ICA presents a promising avenue as a potential therapeutic agent for LUAD.

ICA exhibits significant anti-lung cancer activity. For instance, ICA and its derivatives have been reported to suppress the growth of LC cells and to trigger apoptosis.[22,35] Consistent with previous studies, in this study, we demonstrated that ICA inhibits the growth of A549 cells. This study further demonstrates that ICA can inhibit the growth of lung cancer cells by inducing ferroptosis (Figure 7). Beyond lung cancer, ICA has been shown to modulate ferroptosis in various diseases. For example, it alleviates ferroptosis-related atherosclerosis by promoting autophagy in vascular endothelial cells damaged by xo-LDL and in atherosclerotic mice. ICA inhibits ferroptosis by activating the Nrf2/ARE pathway, thereby alleviating cisplatin-induced premature ovarian failure.[36] Moreover, ICA inhibits ferroptosis in chondrocytes and alleviates osteoarthritis by enhancing SLC7A11/GPX4 signaling.[37] Collectively, these findings suggest that ICA can inhibit lung cancer cell growth through ferroptosis and may exert therapeutic effects in other ferroptosis-related conditions.

TP53 is the most frequently mutated tumor suppressor gene across various cancer types, including LC. In addition to its established role in apoptosis, TP53 plays a crucial part in the regulation of ferroptosis, a process that contributes to the inhibition of lung tumor growth.[38] The activation of TP53 can be triggered by ferroptosis-inducing agents, as demonstrated by the response of the TP53 pathway to oxidative DNA damage induced by erastin in human LUAD A549 cells.[39] Moreover, Cai et.al[38] found that high levels of ROS contribute to ferroptosis induction by triggering lipid peroxidation and activating TP53. Notably, our study revealed that in LUAD, ICA treatment led to an increase in TP53 expression, accompanied by elevated expression levels of ferroptosis-related promotional proteins (ACSL4) and decreased expression levels of inhibitory proteins (GPX4, SLC7A11, FTH1). Our hypothesis suggests that TP53 could facilitate ferroptosis in LUAD cells, necessitating additional experimental confirmation. Interestingly, an African population-specific p53 single nucleotide polymorphism (SNP) leads to a defect in p53-mediated ferroptotic function, thereby impairing its tumor-suppressive role.[40] The role of p53 in ferroptosis is dualistic, and its specific functional direction may depend on the cellular environment, the mutation status of p53, and the cell type.[41]

Cisplatin (CIS) stands out as a widely utilized and potent agent in the treatment of solid tumors.[42] Although numerous cancers show an initial sensitivity to CIS, there is a tendency for tumors to acquire resistance as time progresses, leading to recurrence following additional treatment.[43] Recent investigations have shown that the integration of CIS with

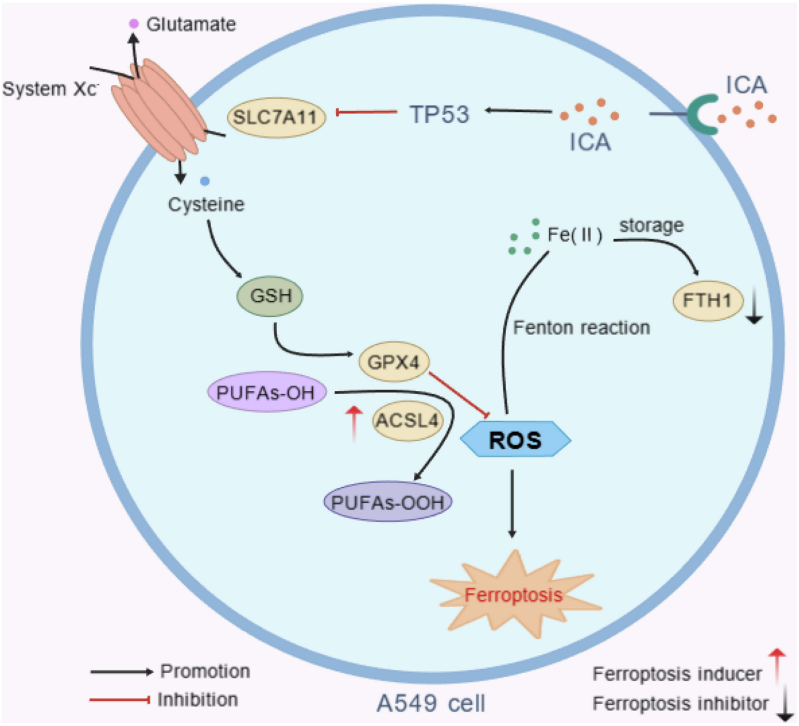

Figure 7 Mechanism diagram of ICA inhibiting lung adenocarcinoma progression. ICA treatment upregulates TP53 expression, which in turn promotes ferroptosis by increasing the expression of the pro-ferroptotic protein ACSL4 and reducing the levels of key anti-ferroptotic markers (GPX4, SLC7A11, and FTH1). ICA exerts anti-tumor effects in LUAD primarily by activating TP53-mediated ferroptosis.

ferroptosis inducers markedly improves antitumor efficacy. For example, the interplay between CIS and the ferroptosis inducer Erastin demonstrates a significant additive impact on tumor suppression,[44] with both ferroptosis and apoptosis playing roles in this amplified effect.[45] Furthermore, it has been demonstrated that ICA enhances the chemosensitivity of OC cells that are resistant to CIS,[46] leading to increased cellular damage and heightened cytotoxic effects induced by CIS.[47–49] The results of our study reinforce these observations, demonstrating that the combination of CIS and ICA significantly hinders tumor growth by activating ferroptosis, which is facilitated by the upregulation of TP53. Furthermore, this combination therapy notably reduced the expression levels of key driver genes associated with LUAD, such as EGFR, KRAS, NRAS, and PIK3CA.

Immunomodulation is essential for sustaining the body's equilibrium. ICA has been shown to modulate immune functions.[50] Increasing data indicates that ICA suppresses tumor growth, invasion, and metastasis via a range of immunomodulatory pathways. These involve augmenting the anti-tumor efficacy of immune effector cells and molecules, inhibiting the tumor microenvironment (TME), and increasing tumor immunogenicity.[51] Research investigations have demonstrated that ICA and its metabolite Icaritin (ICT) can decrease the population of myeloid-derived suppressor cells (MDSCs) while enhancing the ratio of IFN-γ + CD8+ T cells in splenic tissue.[52] Moreover, Hao et al[53] indicated that ICT treatment enhances the TME by facilitating the proliferation of CD8+ T cells in B16 tumor-bearing mice. A separate investigation revealed that the combination of radiotherapy and CIS improves the effectiveness of immunotherapy by stimulating both local and systemic T-cell activity within the TME.[54] These observations align with our results. In our investigation, we noted that ICA prompts the activation of NK T cells, CD4+ T cells, and CD8+ T cells. Given the crucial role of cytotoxic lymphocytes, in effective immunotherapy,[55,56] we suggest that ICA might impede tumor growth by stimulating immune cells.

Our study has several limitations. First, only a single LUAD cell line (A549) was used for verification. To improve the generalizability of these findings, future studies should include at least two LUAD cell lines with distinct genetic backgrounds to minimize potential biases due to cell line specificity. Second, while previous research has shown that icariin can induce apoptosis in lung cancer cells, the present work primarily focused on ferroptosis. It is likely that both

https://doi.org/10.2147/OTT.S539483

apoptosis and ferroptosis contribute to the antitumor effects of ICA. However, the relative contributions of these two pathways were not quantified. Future investigations are warranted to delineate their interplay and clarify the precise mechanisms underlying ICA-induced cytotoxicity. Despite these limitations, our findings suggest that ICA may represent a promising therapeutic candidate for LC treatment by targeting ferroptosis, and could potentially be developed into combination strategies with existing anticancer therapies to enhance efficacy and overcome resistance.

Conclusion

Our results indicate that ICA suppresses the proliferation, migration, and invasion of LUAD cells in a dose-dependent fashion through the activation of TP53-mediated ferroptosis. Moreover, RNA sequencing analysis indicated that ICA enhances the activation of Mø, NK T cells, CD4+ T cells, and CD8+ T cells, concurrently leading to metabolic dysregulation. This research elucidates a possible mechanism for the regulation of ferroptosis in LUAD and offers significant insights into prospective therapeutic approaches for the treatment of LUAD.

Data Sharing Statement

The data that generated or analysed during this study are included in this published article and its supplementary information files. We have submitted the article dataset files on https://www.zenodo.org/record/7634636#. Y-xAe_Lis2w with DOI number 10.5281/zenodo.7634636. Further inquiries can be directed to the corresponding author on reasonable request.

Ethics Approval

In this study, all human data used were obtained from publicly available databases, and the information has been anonymized, without involving any sensitive personal information or commercial interests. According to the national legislation guidelines of China, specifically item 1 and 2 of Article 32 of the Measures for Ethical Review of Life Science and Medical Research Involving Human Subjects (issued on February 18, 2023), which stipulates that: Research using legally obtained public data or data generated through observation without interfering with public behavior is exempt from ethical review; Research using anonymized information and data is exempt from ethical review. Given that our research meets the above circumstances, it is exempt from ethical review approval in accordance with the aforementioned regulations. We confirm that all operations involving human data in this study strictly comply with the relevant national laws, regulations, and ethical norms.

The study was conducted according to the guidelines of the Declaration of Helsinki, and approved by the Animal Ethics Committee of Yunnan Provincial Hospital of Traditional Chinese Medicine (2021012-02, September 14, 2021) and performed in compliance with the National Guidelines for the Care and Use of Animals.

Consent for Publication

All authors have read and agreed to the published version of the manuscript.

Author Contributions

All authors made a significant contribution to the work reported, whether that is in the conception, study design, execution, acquisition of data, analysis and interpretation, or in all these areas; took part in drafting, revising or critically reviewing the article; gave final approval of the version to be published; have agreed on the journal to which the article has been submitted; and agree to be accountable for all aspects of the work.

Funding

This work was supported by Union Research Projects of Yunnan University of Traditional Chinese Medicine [grant number XYLH202050].

Disclosure

The authors declare that they have no competing interests.

References

1. Sung H, Ferlay J, Siegel RL, et al. Global cancer statistics 2020: GLOBOCAN estimates of incidence and mortality worldwide for 36 cancers in 185 countries. *Cancer J Clin*. 2021;71(3):209–249. doi:10.3322/caac.21660
2. Li F, Ge D, Sun S-L. A novel ferroptosis-related genes model for prognosis prediction of lung adenocarcinoma. *BMC Pulm Med*. 2021;21(1):229. doi:10.1186/s12890-021-01588-2
3. Wang Z, Kim J, Zhang P, et al. Current therapy and development of therapeutic agents for lung cancer. *Cell Insight*. 2022;1(2):100015. doi:10.1016/j.cellin.2022.100015
4. Wu S, Zhu C, Tang D, et al. The role of ferroptosis in lung cancer. *Biomarker Res*. 2021;9(1):82. doi:10.1186/s40364-021-00338-0
5. David SE, Douglas EW, Dara LA, et al. Non–small cell lung cancer, version 3.2022, NCCN clinical practice guidelines in oncology. *J National Compr Cancer Network*. 2022;2022:1.
6. Stockwell BR, Friedmann Angeli JP, Bayir H, et al. Ferroptosis: a regulated cell death nexus linking metabolism, redox biology, and disease. *Cell*. 2017;171(2):273–285. doi:10.1016/j.cell.2017.09.021
7. Zheng Q, Wang D, Lin R, et al. Pyroptosis, ferroptosis, and autophagy in spinal cord injury: regulatory mechanisms and therapeutic targets. *Neural Regen Res*. 2025;20(10):2787–2806. doi:10.4103/NRR.NRR-D-24-00112
8. Cheng X, Yu C, Yang X, et al. A panoramic view of ferroptosis in cardiovascular disease. *Kidney Dis*. 2023;9(3):173–186. doi:10.1159/000530046
9. Sheikh A, Kesharwani P, Almalki WH, et al. Understanding the novel approach of nanoferroptosis for cancer therapy. *Nano-Micro Lett*. 2024;16(1):188. doi:10.1007/s40820-024-01399-0
10. Kajarabille N, Latunde-Dada GO. Programmed cell-death by ferroptosis: antioxidants as mitigators. *Int J Mol Sci*. 2019;20(19):4968. doi:10.3390/ijms20194968
11. Rochette L, Dogon G, Rigal E, et al. Lipid peroxidation and iron metabolism: two corner stones in the homeostasis control of ferroptosis. *Int J Mol Sci*. 2022;24(1):449. doi:10.3390/ijms24010449
12. Liu J, Kang R, Tang D. Signaling pathways and defense mechanisms of ferroptosis. *FEBS J*. 2022;289(22):7038–7050. doi:10.1111/febs.16059
13. Chen X, Kang R, Kroemer G, et al. Broadening horizons: the role of ferroptosis in cancer. *Nat Rev Clin Oncol*. 2021;18(5):280–296. doi:10.1038/s41571-020-00462-0
14. Li Y, He X, Ding Y, et al. Statin uses and mortality in colorectal cancer patients: an updated systematic review and meta-analysis. *Cancer Med*. 2019;8(6):3305–3313. doi:10.1002/cam4.2151
15. Yang Z, Zhou Z, Meng Q, et al. Dihydroartemisinin sensitizes lung cancer cells to cisplatin treatment by upregulating ZIP14 expression and inducing ferroptosis. *Cancer Med*. 2024;13(19):e70271. doi:10.1002/cam4.70271
16. He C, Wang Z, Shi J. Pharmacological effects of icariin. *Adv Pharmacol*. 2020;87:179–203.
17. Tao H, Liu M, Wang Y, et al. Icaritin induces anti-tumor immune responses in hepatocellular carcinoma by inhibiting splenic myeloid-derived suppressor cell generation. *Front Immunol*. 2021;12:609295. doi:10.3389/fimmu.2021.609295
18. Wang X, Zheng N, Dong J, et al. Estrogen receptor-α36 is involved in icaritin induced growth inhibition of triple-negative breast cancer cells. *J Steroid Biochem Mol Biol*. 2017;171:318–327. doi:10.1016/j.jsbmb.2017.05.009
19. Li C, Peng W, Song X, et al. Anticancer effect of icaritin inhibits cell growth of colon cancer through reactive oxygen species, Bcl-2 and cyclin D1/E signaling. *Oncol Lett*. 2016;12(5):3537–3542. doi:10.3892/ol.2016.5089
20. Gao L, Chen M, Ouyang Y, et al. Icaritin induces ovarian cancer cell apoptosis through activation of p53 and inhibition of Akt/mTOR pathway. *Life Sci*. 2018;202:188–194. doi:10.1016/j.lfs.2018.03.059
21. Lu PH, Chen MB, Liu YY, et al. Identification of sphingosine kinase 1 (SphK1) as a primary target of icaritin in hepatocellular carcinoma cells. *Oncotarget*. 2017;8(14):22800–22810. doi:10.18632/oncotarget.15205
22. Zhao X, Lin Y, Jiang B, et al. Icaritin inhibits lung cancer-induced osteoclastogenesis by suppressing the expression of IL-6 and TNF-a and through AMPK/mTOR signaling pathway. *Anti-Cancer Drugs*. 2020;31(10):1004–1011. doi:10.1097/CAD.0000000000000976
23. Lu X, Xue B, Zhang T, et al. Down-regulation of microRNA-10a mediates the anti-tumor effect of icaritin in A549 cells via the PTEN/AKT and ERK pathway. *Gen Physiol Biophys*. 2019;38(6):525–533. doi:10.4149/gpb_2019041
24. Song L, Chen X, Mi L, et al. Icariin-induced inhibition of SIRT6/NF-κB triggers redox mediated apoptosis and enhances anti-tumor immunity in triple-negative breast cancer. *Cancer Sci*. 2020;111(11):4242–4256. doi:10.1111/cas.14648
25. Sheng W, Li B, Sun T, et al. Icariin-curcumol promotes ferroptosis in prostate cancer cells through Nrf2/HO-1 signaling. *Exp Ther Med*. 2024;27(5):232. doi:10.3892/etm.2024.12519
26. Wu X, Kong W, Qi X, et al. Icariin induces apoptosis of human lung adenocarcinoma cells by activating the mitochondrial apoptotic pathway. *Life Sci*. 2019;239:116879. doi:10.1016/j.lfs.2019.116879
27. Anders S, Pyl PT, Huber W. HTSeq—a Python framework to work with high-throughput sequencing data. *Bioinformatics*. 2015;31(2):166–169. doi:10.1093/bioinformatics/btu638
28. Love MI, Huber W, Anders S. Moderated estimation of fold change and dispersion for RNA-seq data with DESeq2. *Genome Biol*. 2014;15(12):1–21. doi:10.1186/s13059-014-0550-8
29. Bu D, Luo H, Huo P, et al. KOBAS-i: intelligent prioritization and exploratory visualization of biological functions for gene enrichment analysis. *Nucleic Acids Res*. 2021;49(W1):W317–W325. doi:10.1093/nar/gkab447
30. Kerseviciute I, Gordevicius J, Kelso J. aPEAR: an R package for autonomous visualization of pathway enrichment networks. *Bioinformatics*. 2023;39(11). doi:10.1093/bioinformatics/btad672
31. Hänzelmann S, Castelo R, Guinney J. GSVA: gene set variation analysis for microarray and RNA-seq data. *BMC Bioinf*. 2013; 14(1):7. doi:10.1186/1471-2105-14-7
32. Aaron MN, Chih Long L, Michael RG, et al. Robust enumeration of cell subsets from tissue expression profiles. *Nature Methods*. 2015;2015:1.
33. Yan Y, Teng H, Hang Q, et al. SLC7A11 expression level dictates differential responses to oxidative stress in cancer cells. *Nat Commun*. 2023;14(1):3673. doi:10.1038/s41467-023-39401-9
34. Santarpia M, Aguilar A, Chaib I, et al. Non-small-cell lung cancer signaling pathways, metabolism, and PD-1/PD-L1 antibodies. *Cancers*. 2020;12(6):1475. doi:10.3390/cancers12061475

35. Liu S, Guo Y, Wang J, et al. A novel anticancer agent SNG1153 inhibits growth of lung cancer stem/progenitor cells. *Oncotarget*. 2016;7(29):45158–45170. doi:10.18632/oncotarget.9783
36. Li F, Zhu F, Wang S, et al. Icariin alleviates cisplatin-induced premature ovarian failure by inhibiting ferroptosis through activation of the Nrf2/ARE pathway. *Sci Rep*. 2024;14(1):17318. doi:10.1038/s41598-024-67557-x
37. Xiao J, Luo C, Li A, et al. Icariin inhibits chondrocyte ferroptosis and alleviates osteoarthritis by enhancing the SLC7A11/GPX4 signaling. *Int Immunopharmacol*. 2024;133:112010. doi:10.1016/j.intimp.2024.112010
38. Jiang L, Kon N, Li T, et al. Ferroptosis as a p53-mediated activity during tumour suppression. *Nature*. 2015;520(7545):57–62. doi:10.1038/nature14344
39. Huang C, Yang M, Deng J, et al. Upregulation and activation of p53 by erastin-induced reactive oxygen species contribute to cytotoxic and cytostatic effects in A549 lung cancer cells. *Oncol Rep*. 2018;40(4):2363–2370. doi:10.3892/or.2018.6585
40. Jennis M, Kung C-P, Basu S, et al. An African-specific polymorphism in the TP53 gene impairs p53 tumor suppressor function in a mouse model. *Genes Dev*. 2016;30(8):918–930. doi:10.1101/gad.275891.115
41. Liu Y, Gu W. p53 in ferroptosis regulation: the new weapon for the old guardian. *Cell Death Differ*. 2022;29(5):895–910. doi:10.1038/s41418-022-00943-y
42. Wang D, Lippard SJ. Cellular processing of platinum anticancer drugs. *Nat Rev Drug Discov*. 2005;4(4):307–320. doi:10.1038/nrd1691
43. Amable L. Cisplatin resistance and opportunities for precision medicine. *Pharmacol Res*. 2016;106:27–36. doi:10.1016/j.phrs.2016.01.001
44. Roh J-L, Kim EH, Jang HJ, et al. Induction of ferroptotic cell death for overcoming cisplatin resistance of head and neck cancer. *Cancer Lett*. 2016;381(1):96–103. doi:10.1016/j.canlet.2016.07.035
45. Guo J, Xu B, Han Q, et al. Ferroptosis: a novel anti-tumor action for cisplatin. *Cancer Res Treat*. 2018;50(2):445–460. doi:10.4143/crt.2016.572
46. Jiang S, Chang H, Deng S, et al. Icariin enhances the chemosensitivity of cisplatin-resistant ovarian cancer cells by suppressing autophagy via activation of the AKT/mTOR/ATG5 pathway. *Int J Oncol*. 2019;54(6):1933–1942. doi:10.3892/ijo.2019.4785
47. Liu J, Xie L, Zhai H, et al. Exploration of the protective mechanisms of Icariin against cisplatin-induced renal cell damage in canines. *Front Vet Sci*. 2024;11:1331409. doi:10.3389/fvets.2024.1331409
48. Xia J, Hu J-N, Zhang R-B, et al. Icariin exhibits protective effects on cisplatin-induced cardiotoxicity via ROS-mediated oxidative stress injury in vivo and in vitro. *Phytomedicine*. 2022;104:154331. doi:10.1016/j.phymed.2022.154331
49. Zhou Y-D, Hou J-G, Yang G, et al. Icariin ameliorates cisplatin-induced cytotoxicity in human embryonic kidney 293 cells by suppressing ROS-mediated PI3K/Akt pathway. *Biomed Pharmacother*. 2019;109:2309–2317. doi:10.1016/j.biopha.2018.11.108
50. Li C, Li Q, Mei Q, et al. Pharmacological effects and pharmacokinetic properties of icariin, the major bioactive component in Herba Epimedii. *Life Sci*. 2015;126:57–68. doi:10.1016/j.lfs.2015.01.006
51. Zhangyang B, Wei Z, Xiaoyan Y. Anti-inflammatory and immunoregulatory effects of icariin and icaritin. *Biomed Pharmacother*. 2022;2022:1.
52. Junmin Z, Jinfeng W, Xianghong C, et al. Icariin and its derivative, ICT, exert anti-inflammatory, anti-tumor effects, and modulate myeloid derived suppressive cells (MDSCs) functions. *Int Immunopharmacol*. 2011; 2011:1.
53. Hao H, Zhang Q, Zhu H, et al. Icaritin promotes tumor T-cell infiltration and induces antitumor immunity in mice. *Eur J Immunol*. 2019;49(12):2235–2244. doi:10.1002/eji.201948225
54. Kroon P, Frijlink E, Iglesias-Guimarais V, et al. Radiotherapy and cisplatin increase immunotherapy efficacy by enabling local and systemic intratumoral T-cell activity. *Cancer Immunol Res*. 2019;7(4):670–682. doi:10.1158/2326-6066.CIR-18-0654
55. Hsu J, Hodgins JJ, Marathe M, et al. Contribution of NK cells to immunotherapy mediated by PD-1/PD-L1 blockade. *J Clin Invest*. 2018;128(10):4654–4668. doi:10.1172/JCI99317
56. Borst J, Ahrends T, Bąbała N, et al. CD4+ T cell help in cancer immunology and immunotherapy. *Nat Rev Immunol*. 2018;18(10):635–647. doi:10.1038/s41577-018-0044-0